ACS APPLIED NANO MATERIALS

www.acsanm.org Article

Internalized Hydroxyapatite Nanoparticles Conjugated with a Modified Form of Curcumin Functionalized with Folic Acid Promote Bone Tumor Cell Necrosis

Michele Angela Rodrigues, Jéssica Pauline Nunes Marinho, Luísa Arantes Fernandes Vieira, Dawidson Assis Gomes, and Edésia Martins Barros de Sousa*

Cite This: *ACS Appl. Nano Mater.* 2024, 7, 21304−21318 Read Online

ACCESS | Metrics & More | Article Recommendations | Supporting Information

ABSTRACT: Osteosarcoma (OS) is a common aggressive bone tumor that affects both young adults and children. The prognosis for this type of cancer remains poor due to high lung metastasis rates and radiotherapy resistance. Consequently, the development of innovative strategies to prevent this type of cancer recurrence and metastasis is crucial. This study explored an OS treatment using a modified form of curcumin (CMAP) with hydroxyapatite (CMAP-HA) functionalized with folic acid (CMAP-HAF). The samples were characterized by Fourier transform infrared spectroscopy (FTIR), CHN elemental analysis, ζ-potential, and transmission electron microscopy (TEM). The results showed the successful incorporation of folic acid (FA) into the nanostructure, resulting in cytotoxic effects on osteosarcoma cells (U2OS) and adult human dermal fibroblasts (HDFa). CMAP-HAF treatment decreased cyclin E expression by 16.8 ± 2.3%. Furthermore, CMAP-HAF was internalized by 99.6% of U2OS cells, compromising plasma membrane integrity, causing necrosis, affecting cell migration and cloning formation. These findings suggest that CMAP-HAF is a promising therapeutic agent for OS treatment and offers an innovative approach to improve patient outcomes.

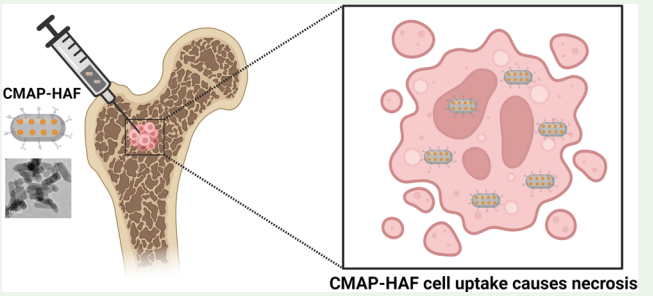

KEYWORDS: *osteosarcoma, curcumin nanocomposites, hydroxyapatite, folic acid, necrosis, cellular uptake*

1. INTRODUCTION

Osteosarcoma (OS) is the second most common type of primary malignant bone tumor and is highly aggressive.[1,2] This type of cancer has a poor prognosis because lung metastasis is developed by about 30% of patients.[1] Moreover, identifying a targeted treatment for OS is challenging due to the high frequency of gene mutations.[3,4] Therefore, developing new strategies to prevent cancer metastasis and recurrence is essential for ongoing research. In this context, bionanomaterials have been widely used in biomedical research for numerous applications.

Hydroxyapatite (HA), a key natural component of bone, has been extensively used as a biomaterial owing to its potential biomedical applications. Their superior biocompatibility makes them a popular choice for bone repair.[5,6] Additionally, recent reports have suggested that nanoparticles of this substance can suppress the proliferation of several cancer cells.[7] Furthermore, HA nanoparticles have been reported to accelerate bone fracture healing via local delivery and controlled release of microRNAs.[8] Previous research has shown that treatment with these nanoparticles can reduce cell proliferation by promoting apoptosis in OS cell lines,[9] melanoma,[10] gastric cancer,[11] glioma,[12] and breast cancer.[13] The specific effects appear to vary by cell type, for example, by supporting the proliferation of osteoblasts while triggering apoptosis of OS cells.[5]

Another compound explored for OS treatment is curcumin (CM), which can be extracted from *Curcuma longa*. It exhibits a range of pharmacological effects, including anti-inflammatory, antioxidant, and antitumor properties, via modulation of intracellular signaling pathways that regulate cell proliferation, inflammation, and cell death.[1,14] The antitumor effects of this compound have been explored in several types of tumors, including prostate, colon and breast cancer.[15,16] Another notable property of this substance is its ability to repair bone defects caused by tumor invasion or surgical procedures.[17] Furthermore, CM has been reported to be an option for OS therapy by suppressing OS development while repairing bone defects.[1,18] The combination of CM with folic acid (FA) (vitamin B9) has also been reported to improve bioavailability

Received: April 29, 2024
Revised: August 27, 2024
Accepted: September 2, 2024
Published: September 10, 2024

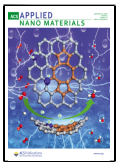

https://doi.org/10.1021/acsanm.4c02467
ACS Appl. Nano Mater. 2024, 7, 21304−21318

and efficacy in treating diseases, such as cervical cancer.[19] Curcumin conjugated with FA reduced the tumor volume in Balb/c nude mice without causing body weight loss. These results indicate that CM with FA remarkably decreases tumor growth.[20] The process of functionalizing HA nanorods with aminated folate, without using a coat or polymeric ligand, results in a stable material with robust interactions between folate and nanorod surfaces.[21]

The combined effect of HA, a modified form of CM, and FA on OS cells has not been investigated. This study explored the synthesis, characterization, and biological properties of a new HA system with APTES-modified CM, CMAP-HA, and its functionalization with FA (CMAP-HAF) for OS treatment. This research opens a new avenue in nanomedicine, potentially improving the treatment of OS by introducing a novel, highly effective, and biocompatible system, CMAP-HAF, which could significantly enhance the efficacy of current treatment modalities.

2. MATERIALS AND METHODS

2.1. Materials. All chemicals listed below were sourced from Sigma-Aldrich unless otherwise referenced. Hexadecyltrimethylammonium bromide (CTAB; $C_{14}H_{42}N{\cdot}Br$), calcium nitrate tetrahydrate, $Ca(NO_3)_2{\cdot}4H_2O$, dibasic potassium phosphate trihydrate, $K_2HPO_4{\cdot}3H_2O$, ammonium hydroxide (NH_4OH), curcumin (CM), 3-aminopropyltriethoxysilane - APTES, folic acid, and acetic acid P.A. (Neon).

2.2. Synthesis of Hydroxyapatite Nanorods. A surfactant-assisted hydrothermal method was used to synthesize hydroxyapatite nanorods, as described in detail by Marinho et al.[22]

2.3. Synthesis of CMAP-HA Nanostructures. To introduce CM into HA, a modified form of CM was created.[22] This was achieved by reacting 1 mmol of CM and 4 mmol of APTES in an acidic solution at 75 °C for 24 h with continuous stirring using a reflux system in an inert atmosphere. Next, the solution was lyophilized for 48 h at 1.65 mbar pressure at −85 °C to obtain the material in powder form (freeze-dryer Christ α 2−4 LSCbasic). HA and CMAP were mixed at a 1:1 ratio by mass in 50 mL of deionized water and stirred for 24 h at 50 °C. The resulting material was filtered, washed with water, and dried at 60 °C for 24 h. The resulting nanostructure was called CMAP-HA.

2.4. Functionalization Process of CMAP-HA Nanostructures with Folic Acid. CMAP-HA and FA were mixed at a mass ratio of 1:1 in 50 mL of deionized water. The mixture was then stirred vigorously for 24 h at 50 °C. The obtained powder was gathered by vacuum filtration, then washed with water and dried at 60 °C for 24 h. The final product was named as CMAP-HAF.[21,22]

2.5. Labeling of Synthesized Nanoparticles with Fluorescein (FITC). To conjugate the nanoparticles with FITC, 50 mg of the HA sample and 50 mg of CMAP-HAF were mixed individually with FITC (2.7 mg) in 7 mL of 15% (v/v) alcoholic solution, as previously described by Meireles et al.[23]

2.6. Nanoparticles Characterization. The morphology of the nanoparticles was assessed by images acquired by transmission electron microscopy (TEM) using Tecnai G2−20 FEI SuperTwin 200 kV equipment (FEI Company) from *Centro de Microscopia* (UFMG). The samples were dispersed in deionized water using tip ultrasound (10 kj) and a drop of the suspension was deposited into a Formvar/carbon film sample holder with 300 mesh copper (Electron Microscopy Sciences). Fourier transform infrared (FTIR) was used to examine the characteristics of the functional groups of the samples. Infrared spectra in the wavelength range of 4000 to 400 cm^{-1} were obtained by the Bruker instrument model Vertex 70v (Bruker), using a Platinum Diamond ATR in vacuum with a resolution of 4 cm^{-1} at 128 scans min. Chemical modifications were investigated using CHN on an EA 2400 CHNS/O analyzer (PerkinElmer). ζ-Potential was executed using Nanozetasizer Zs (Malvern Instruments, U.K.). The measurements were performed as previously described.[22−24]

2.7. Cell Culture. Osteosarcoma U2OS cells and adult human dermal fibroblasts (HDFa) were purchased from ATCC and Life Technologies (Carlsbad, CA), respectively. Cells were cultured in an incubator at 37 °C in a 5% CO_2 atmosphere as previously described.[24]

2.8. MTT and Nuclear Cell Counting Assays. Cell viability was assessed using the tetrazolium salt 3-(4, 5-dimethylthiazol-2-yl)-2, 5-diphenyl tetrazolium bromide (MTT) assay, and cell proliferation was used to investigate the viability of HA and CMAP-HAF nanorods.[23] For the MTT assay, HDFa and U2OS cells were seeded (2.0×10^4 cells/well) in 96-well plates. After 24 h of incubation (37 °C, 95% humidity, and 5% CO_2), the cells were treated with nanomaterials (5, 10, 50, and 100 $\mu g\ mL^{-1}$). The MTT and nuclear cell counting assays were performed as previously described.[23,24] The images were taken at 10 random areas per group by an inverted fluorescence microscope EVOS-FL (Thermo Scientific). Experiments were made in triplicate. Cell counting was evaluated using the ImageJ software (https://imagej.nih.gov/ij/). In brief, we used a plugin to automatically count the cells, as described by Grishagin.[25]

2.9. Reactive Oxygen Species (ROS) Assay. Intracellular ROS levels were evaluated using carboxy-H2DCFDA [5-(6)-carboxy-2′,7′-dichlorodihydrofluorescein]; (Thermo Scientific).[26] HDFa and U2OS cells were seeded in 96-well plates at a density of 2×10^4 cells/well and were incubated at 37 °C for 24 h. The cells were then treated with the nanomaterials (5, 10, 50, and 100 $\mu g\ mL^{-1}$) for 48 h. As a positive control, 300 μM of H_2O_2 was used for 2 h to induce ROS. The cells were then washed with phosphate buffered saline (PBS) and stained with 25 μM carboxy-H2DCFDA for 30 min, followed by another wash with PBS. The fluorescence was measured using a Synergy 2 microplate reader (BioTek Instruments, Inc.).

2.10. Western Blot. Western blotting was performed as described by De Miranda et al.[27] In brief, U2OS cells were plated in a 60 mm culture dish and treated for 48 h with HA or CMAP-HAF (100 $\mu g\ mL^{-1}$). Next, the cells were washed with PBS (Thermo Scientific), harvested by scraping, and lysed in NETN buffer (150 mM NaCl, 1 mM EDTA, 20 mM Tris-HCl, pH 8.0, and 0.5% Nonidet P-40). Protease inhibitors (Sigma-Aldrich) were added to the buffer. The total cell lysates were incubated on ice for 10 min. The homogenate was centrifuged at 16,100*g* for 20 min at 4 °C. Proteins were quantified using the Bradford assay (Sigma-Aldrich). The primary antibodies used were mouse monoclonal anticyclin E clone HE12 (1:1000; Invitrogen, cat. 321600), rabbit monoclonal anticyclin D1 clone SP4 (1:1000; Invitrogen, cat. MA5−14512), and rabbit polyclonal anti-CDK1 (1:1000; Invitrogen, cat. no. PA5−82086). The membranes were developed using the SuperSignal West Pico PLUS Chemiluminescent Substrate (Thermo Scientific). Subsequently, the films were scanned and analyzed using the ImageJ software.

2.11. Flow Cytometry. HDFa and U2OS cells were seeded in 6-well culture plates at a density of 2×10^5 cells/well and incubated for 24 h. Next, the cells were incubated with HA or CMAP-HAF at the calculated IC_{50} or 100 $\mu g\ mL^{-1}$ for 24 h. As a positive control for apoptosis, U2OS and HDFa cells were incubated with 10 μM or 500 nM staurosporine for 24 h, respectively. The cells were then removed, centrifuged, and stained using an Annexin V-Alexa Fluor 488 Apoptosis Kit and 7-aminoactinomycin D (7-AAD; Thermo Scientific) for 15 min. The cells were analyzed using a Guava easyCyte 6−2 L Flow Cytometer (Millipore). Annexin V-Alexa Fluor 488 was excited with a 488 laser and the emission was acquired with a 525:30 filter. The 7-AAD signal was collected using a 633 laser and 690:50 emission filter. Fluorescence was compensated before data collection and FlowJo was used for data analysis (Tree Star). Flow cytometry was also used for the internalization assay in cells treated with HA and FITC-conjugated CMAP-HAF.[28,29]

2.12. Cellular Uptake by Immunofluorescence. HDFa and U2OS cells were seeded at 2×10^5 cells per 35 mm dish 24 h before the assay. FITC-labeled nanoparticles diluted in DMEM at 100 $\mu g\ mL^{-1}$ were added to each dish for 24 h at 37 °C. After washing twice with PBS, 1 mL of ice-cold methanol was added for 10 min to fix the cells on the coverslip. The cells were then washed once with PBS, and 1 mL of 0.5% Triton X-100 solution in PBS was added to

https://doi.org/10.1021/acsanm.4c02467
ACS Appl. Nano Mater. 2024, 7, 21304−21318

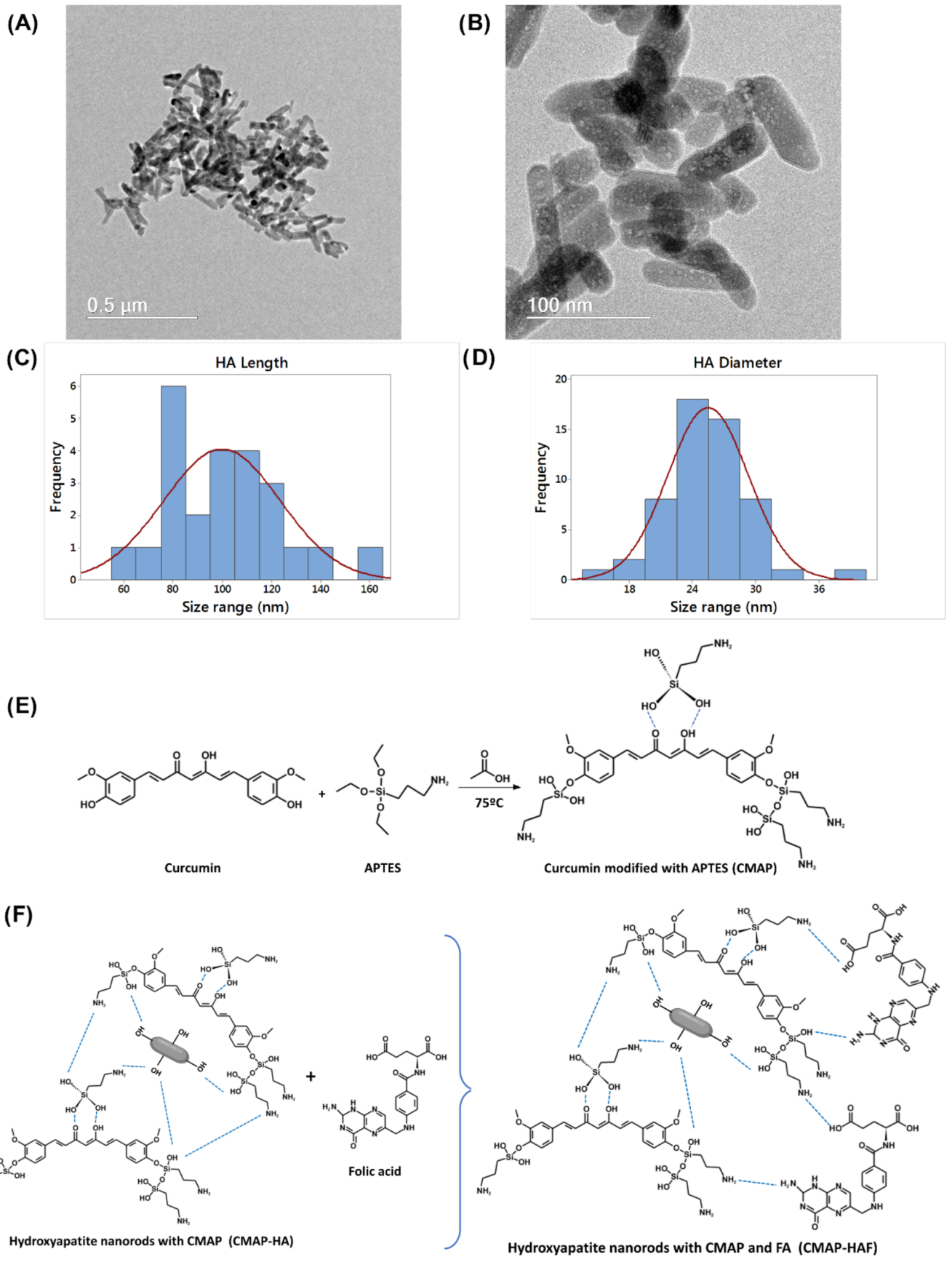

Figure 1. Representative TEM photomicrographs and nanoparticle chemical reaction scheme. (A) The left image represents a low-magnification image of the HA nanoparticles (scale bar = 0.5 μm). (B) The image on the right shows high magnification of the HA nanoparticles (scale bar = 100 nm). (C, D) Nanoparticle size distribution. (E) Chemical modification of CM with APTES. (F) Representative interactions between HA, CMAP, and FA.

https://doi.org/10.1021/acsanm.4c02467
ACS Appl. Nano Mater. 2024, 7, 21304−21318

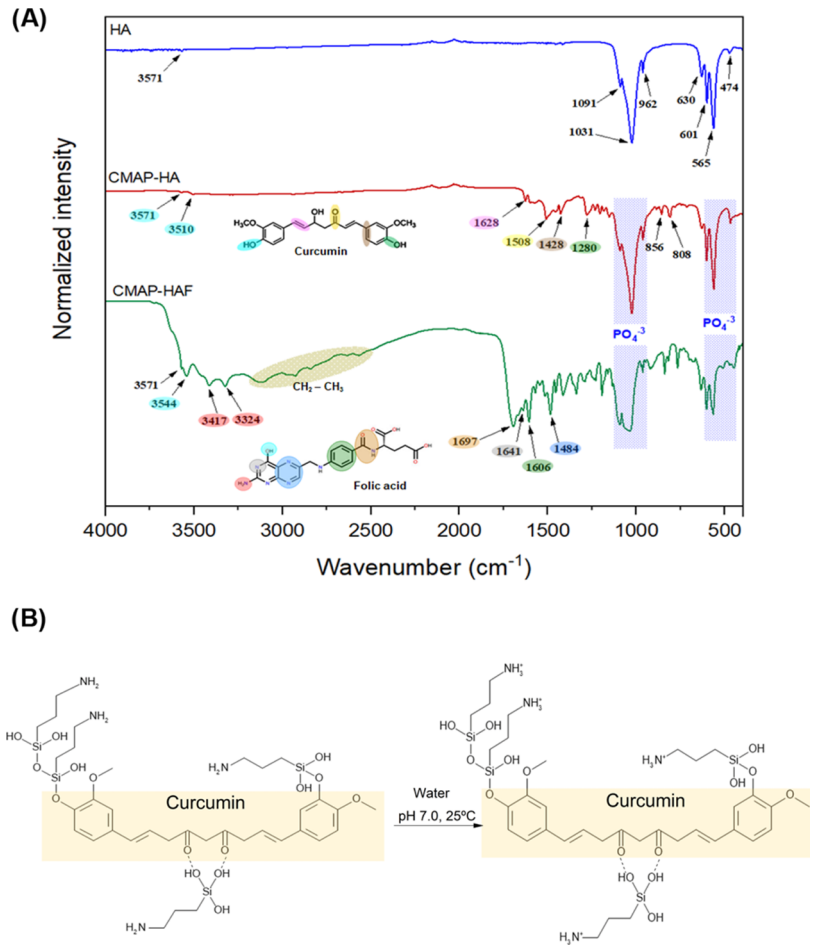

Figure 2. FTIR spectra and schematic of folate-amination interactions. (A) FTIR spectra comparison of HA, CMAP-HA, and CMAP-HAF samples; (B) Schematic illustration of the folate amination interaction.

permeabilize the cells for 10 min. Next, the cells were incubated overnight at 4 °C with a mouse monoclonal anti-α-tubulin antibody (clone DM1A, 1:200) and then incubated with Alexa Fluor 546 (1:1000, Thermo Scientific). Hoechst 33342 (2 μg mL^{-1}, Thermo Scientific) was used as the nuclear marker. A negative control was included in all reactions, including untreated cells, and the primary antibody was omitted. Images were collected using a Leica GSD/TIRF HP microscope with a 63×, 1.43 NA oil objective lens. The images were deconvoluted using LAS X software using 10 interactions.[23,27,30]

2.13. Scratch Assay. Cellular migration was assessed using a wound healing assay as previously described[31] In brief, cells were plated at 2 × 10^5 cells/well in a 24-well dish for 24 h and then a scratch was made by displacing cells using a 200 μL tip (Sarstedt). After scratching, the cells were washed with PBS, incubated with DMEM, and treated with HA or CMAP-HAF nanomaterials (100 μg mL^{-1}). The scratched area was imaged using a 4× objective and a QIClick camera (QImaging) installed on an IX70 Olympus inverted microscope (Olympus) using Image-Pro Plus software (Media Cybernetics) after wounding for 0, 24, or 48 h. Cell migration was measured using ImageJ software, as previously described.[32,33]

2.14. Clonogenic Assay. One thousand U2OS cells were plated in each well of a 6-well plate for 18 h. Cells were then treated with HA or CMAP-HAF (10.4 or 100 μg mL^{-1}) for 48 h, washed with PBS, and left to recover in fresh media for 8 days. The cells were then fixed in 100% ice-cold methanol for 20 min and stained with 0.5% Crystal Violet (Sigma-Aldrich) for 20 min. Colonies were counted using ImageJ.[34]

2.15. Statistical Analysis. All experiments were performed in triplicate, and the data are presented as the mean ± SD. Data were analyzed using GraphPad Prism 9, Microsoft Excel and Minitab. Differences between experimental groups were assessed for significance using One-way analysis of variance (ANOVA) analysis of variance. Statistical significance was set at least $p < 0.05$.

3. RESULTS AND DISCUSSION

3.1. Transmission Electron Microscopy. The morphological characterization of the nanoparticles was performed using TEM. The resulting images are shown in Figure 1A,B. The synthesized hydroxyapatite exhibited a porous structure with a nanorod-like morphology. These nanorods exhibited a nonuniform size distribution, as shown in the graphs (Figure 1C,D). A total of 65 particles were measured for statistical analysis, which indicated an average length of 96.1 ± 24.7 nm and an average diameter of 25.4 ± 3.8% nm. Figure 1E,F shows a representative scheme of the CM and APTES chemical modifications and HA interaction with CMAP and FA molecules. The size distribution of the nanorods was similar to that reported in our previous study.[22] Chen et al. examined HA nanoparticles that were 100 nm in length and 20 nm in diameter.[35] Furthermore, Wu et al. showed that the nano-HA size range, from 100 to 200 nm, is desirable for candidate nanomaterials to act as cancer treatment agents since they accumulate spontaneously in solid tumors by the increased retention effect (EPR) and permeability.[36]

3.2. Fourier Transform Infrared Spectroscopy. The FTIR spectra of pure HA, functionalized CMAP-HA, and

https://doi.org/10.1021/acsanm.4c02467
ACS Appl. Nano Mater. 2024, 7, 21304−21318

CMAP-HAF nanoparticles showed vibrational modes of the functional groups characteristic of hydroxyapatite (Figure 2A). The bands recorded at 1091, 1031, 962, 630, 601, 565, and 474 cm^{-1} were attributed to the fingerprint regions of the stretching and bending vibrations of the phosphate group.[22,37−39] The bands at 1091 and 1031 cm^{-1} were attributed to the asymmetric axial strain vibration, whereas the band at 962 cm^{-1} was due to the symmetric axial strain.[40] The vibrational modes at 565 and 474 cm^{-1} are attributed to the symmetric and asymmetric angular deformation of the P−O−P bond.[41] The bands recorded at 3571 and 630 cm^{-1} were attributed to the stretching and bending vibrations of hydroxyl HA.[42]

In the CMAP-HA sample spectrum, in addition to the bands associated with phosphate, it was possible to observe the presence of bands characteristic of CM. The band detected at 1508 cm^{-1} corresponds to the exclusive axial deformation of the carbonyl, while the band at 1628 cm^{-1} corresponds to the superposition of the vibrational modes of the axial deformation of the carbonyl C═O bond, the C═C bond, and aromatic ring bonds. The band at 1280 cm^{-1} is due to the vibration of the C−O bond of the enol group.[43,44] The in-plane angular deformation vibrations of the aromatic C−C−C ring, C−C−H, and C−O−H bonds were attributed to the band at 1429 cm^{-1}[45] The bands at 856 and 808 cm^{-1} are related to the out-of-plane angular deformation vibrations of the aromatic ring (C−C−H). The band at 3503 cm^{-1} is associated with the axial deformation of the phenolic hydroxyl.[46]

In the spectral analysis of the CMAP-HAF nanostructure, it was not feasible to discern bands indicative of the presence of CM, which was likely attributable to the superimposition of the vibrational modes of the functional groups of FA. The bands observed at 1697, 1645, 1605, and 1481 cm^{-1} were associated with the amide group, axial distortion of the benzene ring, angular deformation of the NH bond, and axial deformation of the heteroring.[47] A schematic illustration of the folate-amination interaction is shown in Figure 2B.

3.3. CHN Elemental Analysis. Chemical modifications by the addition of an organic phase were investigated using CHN.[24] The results of the elemental analysis (Table 1) showed an increase in the percentage of carbon in the CMAP-HA and CMAP-HAF samples compared to that in HA. This gradual increase was associated with the presence of this element in the chemical composition of CM and FA. A similar increase was observed in the nitrogen content of the sample. In the CMAP-HA sample, nitrogen was associated with the APTES used to modify the CM, as it has amine groups in its structure. After incorporating FA, an even greater increase in nitrogen content was observed because of the large amount of the element present in the pterin ring and the *p*-amino benzoic acid portions of the FA structure.[47] The increasing amount of carbon from HA to CMAP-HA and CMAP-HAF (0.6 to 19.8 and 32.6%, respectively) and nitrogen (0.4 to 0.9 and 9.9%, respectively) suggests the presence of FA on the surface of the sample, indicating the incorporation efficiency. Previous work has demonstrated the direct functionalization of HA with FA using aminated FA.[21] Moreover, a higher FA deposition on the HA nanoparticles was observed, indicating increased group functionalization. Therefore, FA conjugation to nanostructures has been shown to improve the delivery of therapeutic agents.[48]

Table 1. Elemental Analysis Results for HA, CMAP-HA, and CMAP-HAF Samples

samples	%C	%H	%N
HA	0.6	0.1	0.4
CMAP-HA	19.8	1.5	0.9
CMAP-HAF	32.6	2.7	9.9

3.4. ζ-Potential Analysis. ζ-Potential measurements are important in determining particle surface properties.[23] It determines the particle stability to study the surface charges anchored in the nanomaterials and defines the potential interactions of the nanomaterials with the cellular plasma membrane.[49] Most particles dispersed in an aqueous medium have a surface charge that results from the dissociation of functional groups on their surfaces. By observing the ζ-potential of the synthesized samples, presented in Table 2, it is possible to verify a significant change in the values attributed to the functionalization process. The ζ-potential of HA changed from −18.5 to +15.3 mV after CMAP incorporation. This change can be attributed to the protonation of the amine groups in the APTES molecule used to modify CM, as illustrated in Figure 2B. After the addition of FA, the ζ-potential value undergoes a further change to −9.9 mV, possibly due to the presence of the carboxylate anion formed by the deprotonation of the carboxyl groups. The changes in ζ-potential values allowed us to infer that the functionalization process promoted significant changes on the surface of the nanoparticles. Other studies have reported that the nanoparticles cellular uptake is significantly influenced by their morphology, size, and surface charge.[20] For instance, Yin et al. reported that hepatoma cells can effectively uptake negatively charged HA nanoparticles.[50] Electronegative nanoparticles can be internalized by cells through endocytosis after nonspecific adsorption to the positively charged regions of the cell membrane.[49]

Table 2. ζ-Potential Measurements of HA, CMAP-HA, and CMAP-HAF Samples

samples	ζ-potential (mv) ± SD
HA	−18.5 ± 2.4
CMAP-HA	+15.3 ± 0.8
CMAP-HAF	−9.9 ± 0.4

3.5. Cell Counting and Viability. The antitumor properties of CM and FA have been investigated in various cancer types.[1,51] In this study, a unique blend of CMAP and FA (CMAP-HAF) was used as a potential candidate for OS treatment. MTT assay was performed to evaluate nanomaterial cytotoxicity. Furthermore, cell counting was employed to ascertain the potential of CMAP-HAF as a viable candidate for OS therapy.

First, HDFa cells treated with 50 and 100 $\mu g\ mL^{-1}$ of CMAP-HAF showed a decrease in cell number of 104.9 ± 19.11 and 124.6 ± 19.11 cells/mm^2, respectively ($p < 0.0001$, Figure 3A). Furthermore, cells treated with 50 and 100 $\mu g\ mL^{-1}$ of CMAP-HAF reduced cell viability by 39.86 ± 3.7 and 53.44 ± 3.7%, respectively ($p < 0.0001$, Figure 3C). HA treatment did not affect HDFa cell count or viability (Supporting Figure S1A−C).

In addition, U2OS cells treated with CMAP-HAF showed a reduction in the number of cells to 10 (114.8 ± 42.29 cells/mm^2), 50 (201.8 ± 42.29 cells/mm^2), and 100 (249.7 ± 42.29

https://doi.org/10.1021/acsanm.4c02467
ACS Appl. Nano Mater. 2024, 7, 21304−21318

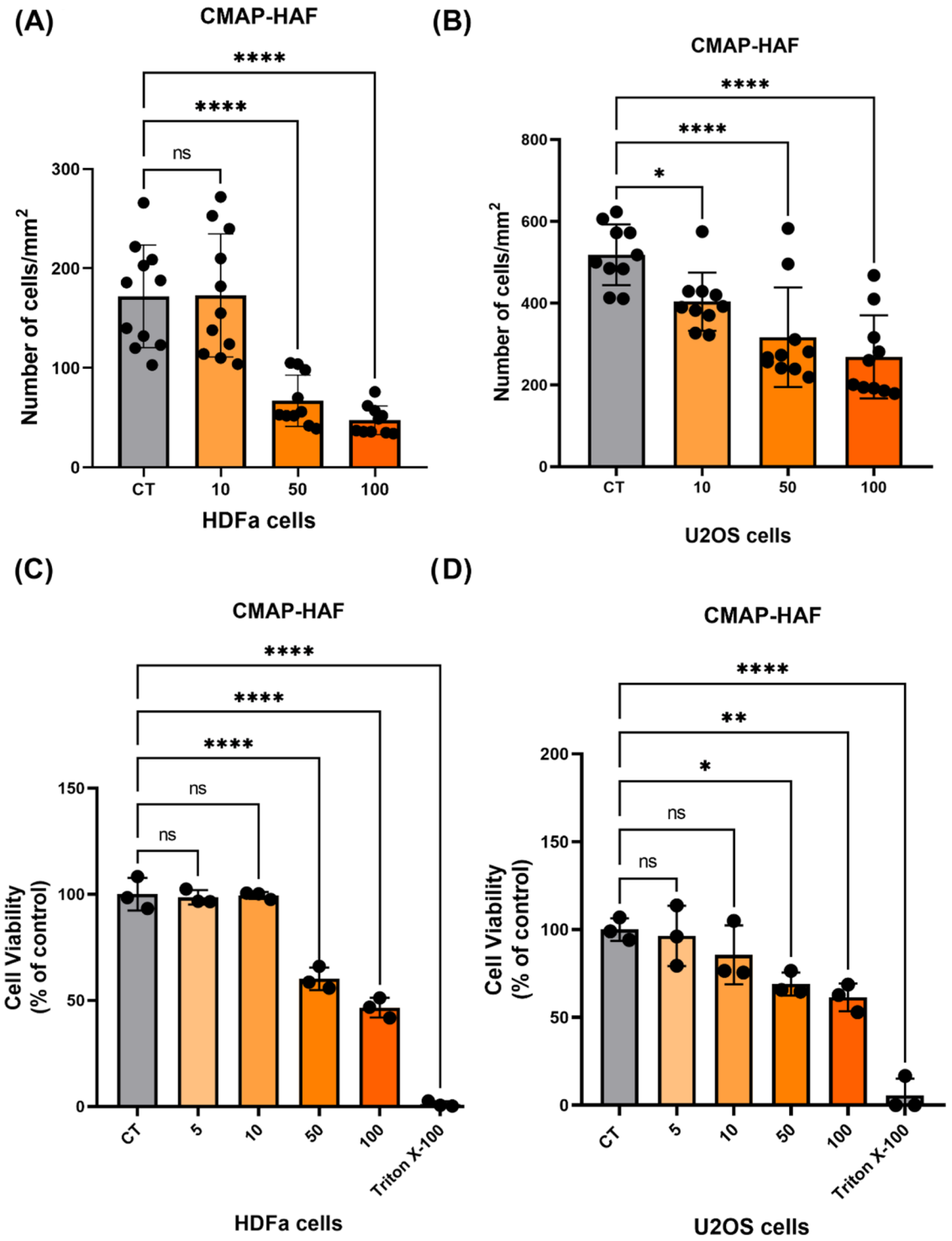

Figure 3. A high dose of CMAP-HAF caused cytotoxicity in HDFa and U2OS cells. The cells were treated with CMAP-HAF at concentrations of 5, 10, 50, or 100 μg mL^{-1}. (A, B) HDFa and U2OS nuclear cell counting in each group was performed using Hoechst staining (see Supporting Figures S2 and S3). The graph illustrates cell density (cells/mm^2) across 10 images per group. (C, D) Bar graphs represent MTT data expressed as a percentage relative to the control group (CT) of HDFa and U2OS cells treated with CMAP-HAF. Cells incubated with Triton-X 100 served as the positive controls. ns = not significant. * $p < 0.05$, ** $p < 0.01$, **** $p < 0.0001$.

cells/mm^2) μg mL^{-1} ($p < 0.0001$, Figure 3B). The viability of U2OS cells was significantly decreased by 50 (31.05 ± 9.5%) and 100 (38.56 ± 9.5%) μg mL^{-1} CMAP-HAF ($p < 0.0001$, Figure 3D). This reduction was dose-dependent and the calculated IC_{50} was 10.4 μg mL^{-1} (Supporting Figure S4). Our previous work using CMAP-HA without FA functionalization demonstrated reduced cell viability and number of cells only at higher concentrations (50 or 100 μg mL^{-1}).[22] Next, we tested whether the nanomaterials could induce cellular ROS production. However, no difference was observed under HA or CMAP-HAF treatment in HDFa and U2OS cells (Supporting Figure S5A–D).

In conclusion, HDFa and U2OS cells showed significantly reduced cell count and viability when treated with high doses

https://doi.org/10.1021/acsanm.4c02467
ACS Appl. Nano Mater. 2024, 7, 21304−21318

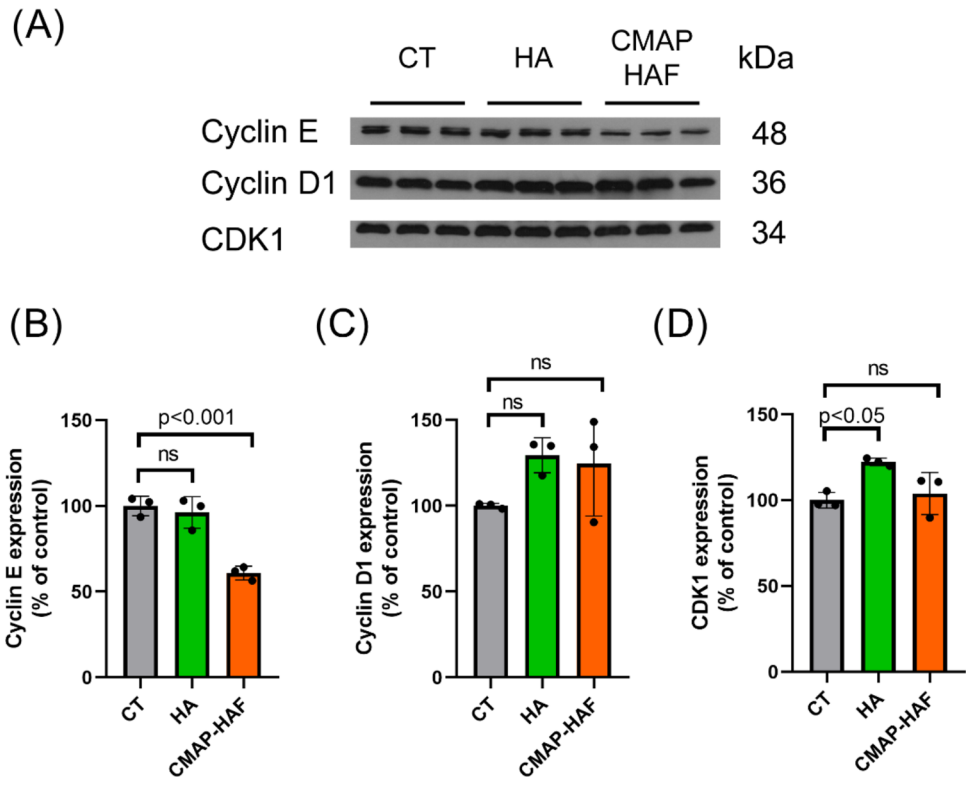

Figure 4. CMAP-HAF decreased cyclin E expression in U2OS cells. (A) Western blot analysis of cyclin E, cyclin D1 and CDK1 after HA or CMAP-HAF treatment in U2OS cells. (B–D) Representative graphs show the protein expression (% of control) of cells treated with HA or CMAP-HAF, demonstrating a decrease in cyclin E but no difference in cyclin D1 and CDK1 expression. Experiments were performed in triplicate (ns = not significant).

of CMAP-HAF, indicating their potential cytotoxic effects. The reduction in cell viability was dose-dependent in the U2OS cells. Cell counting using 10 μg mL^{-1} of CMAP-HAF decreased only in U2OS cells (Figure 3B). This finding emphasizes the possibility of potent effects of CMAP-HAF on this OS cell line. These findings suggest that FA functionalization of CMAP-HAF plays a crucial role in its cytotoxic effects.

Calcium phosphate-based materials such as HA can be used as nanocarriers for CM delivery to offer a platform for the controlled release of CM-based nanostructures to the targeted tumor site.[52] In this study, HA alone did not cause cytotoxicity. However, it has been reported that HA nanoparticles exert cytotoxic effects on tumor cells, such as human hepatoma, colon, and gastric cancer.[52] Lee et al. showed that HA modified with carboxylic acid groups exhibited higher antiproliferative activity and time-dependent cellular uptake of CM nanocomposites in breast cancer cells (MCF-7) than unmodified HA.[53] Radha et al. demonstrated that free CM treatment increased cytotoxicity in HCC 1954 cells and reduced cell proliferation with increasing curcumin concentration.[54] Furthermore, FA conjugation has been reported to improve the nanoparticle bioavailability.[19] In the present study, CMAP-HAF exhibited a dose–response effect only in the U2OS cells. This observation underlines the potential cell line specificity of CMAP-HAF in this OS cell line. Further studies are necessary to investigate the mechanisms underlying this difference in the action of CMAP-HAF in U2OS cells. Such insights will enhance our understanding of the mode of action of CMAP-HAF and pave the way for its optimized use in various cellular contexts.

3.6. Cell Cycle Analysis. To examine the progression through the cell cycle, as preliminary data from nuclear cell counting indicated a decrease in the number of cells, the protein expression of cell cycle checkpoint proteins such as cyclins and cyclin-dependent kinases was investigated.[55] These proteins ensure that each phase of the cell cycle is completed before the next phase begun.[56] To determine whether HA or CMAP-HAF treatment specifically affected the G1/S and G2/M transition, the expression of checkpoint proteins cyclin D1, cyclin E, and cyclin-dependent kinase CDK1 was studied by Western blot analysis. The expression levels of cyclin D1 and CDK1 (Figure 4A–D) were unchanged upon HA or CMAP-HAF treatment compared with the untreated control group. However, the expression of cyclin E decreased by 16.8 ± 2.3% (Figure 4A,B). Together, these observations suggest that CMAP-HAF reduced the expression of the cell cycle checkpoint protein cyclin E, which is a regulator of the G1/S phase during cell proliferation. Cyclin E is a regulatory protein involved in cell cycle progression. It forms complexes with cyclin-dependent kinase 2 (CDK2) and promotes the transition from G1 to S phase of the cell cycle. Zhou et al. showed that CM treatment promoted cell cycle arrest in acute myeloid leukemia (AML)[57] In our study, its downregulation may be a potential therapeutic target for cancer treatment by inhibiting cancer cell growth. However, cyclin E inhibition remains unclear, and further investigation is necessary.

3.7. Annexin V and 7-AAD Analysis by Flow Cytometry. The possible apoptotic or necrotic effects of CMAP-HAF treatment were investigated in U2OS and HDFa cells using flow cytometry.[28,29] Apoptosis and necrosis were measured using Annexin V Alexa-488 and 7-AAD, respectively.

https://doi.org/10.1021/acsanm.4c02467
ACS Appl. Nano Mater. 2024, 7, 21304–21318

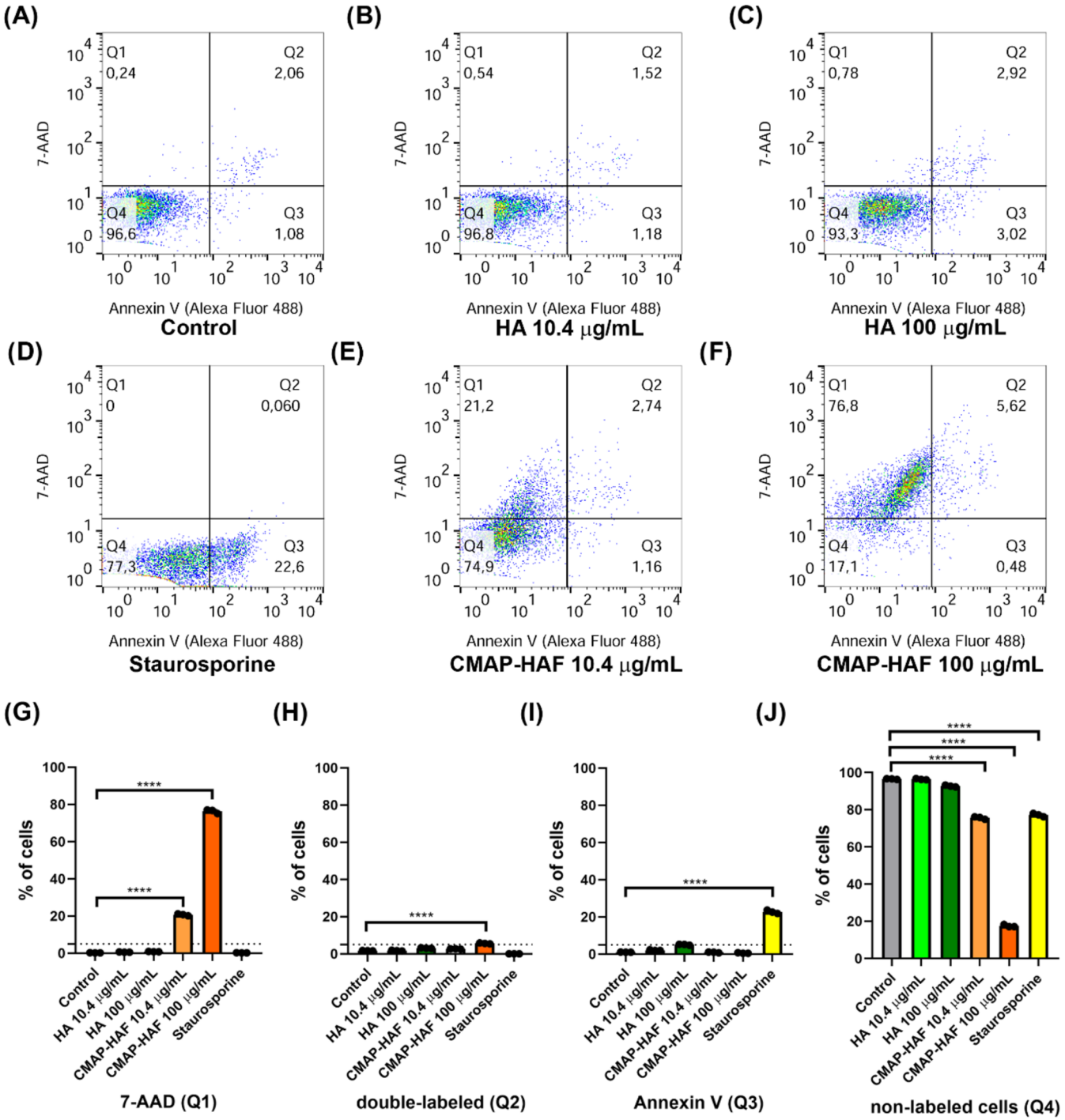

Figure 5. CMAP-HAF causes necrosis in U2OS cells. U2OS cells were incubated with 7-AAD and annexin V and analyzed using flow cytometry. (A–F) Cells stained with 7-AAD but not with Annexin-V dye are necrotic cells, and they are presented in quadrant Q1 (top left). Cells positive for Annexin-V and 7-AAD were necrotic and apoptotic and quadrant Q2 (top right). Cells stained with Annexin V and not with 7-AAD were apoptotic cells (quadrant Q3, bottom right). Cells that did not stain for either 7-AAD or Annexin-V dye were nonapoptotic and non-necrotic (live cells), quadrant Q4 (bottom left). Each experiment was performed in triplicate. (G–J) Graphs quantifying the percentage of events in each quadrant. The graphs are representative of three independent experiments (**** $p < 0.0001$).

Disruption of cell membrane phospholipid asymmetry, leading to the exposure of phosphatidylserine on the cell surface, is an early indicator of apoptosis. Fluorescently labeled annexin-V specifically binds to these externalized phosphatidylserine molecules, enabling the detection of apoptotic cells. 7-AAD is a fluorescent membrane-impermeant dye that binds to double-stranded DNA in membrane-compromised cells, whereas DNA in healthy cells remains unstained.[58] First, cells were exposed to HA or CMAP-HAF using 10.4 μg mL^{-1} (EC_{50}) or 100 μg mL^{-1} of the nanoparticles.

First, it was observed that untreated and HA-treated U2OS cells with HA do not exhibit Annexin-V Alexa-488 or 7-AAD labeling (Figure 5A–C,5G–I). However, U2OS treated with 10.4 μg mL^{-1} (EC_{50}) or 100 μg mL^{-1} of CMAP-HAF were

https://doi.org/10.1021/acsanm.4c02467
ACS Appl. Nano Mater. 2024, 7, 21304–21318

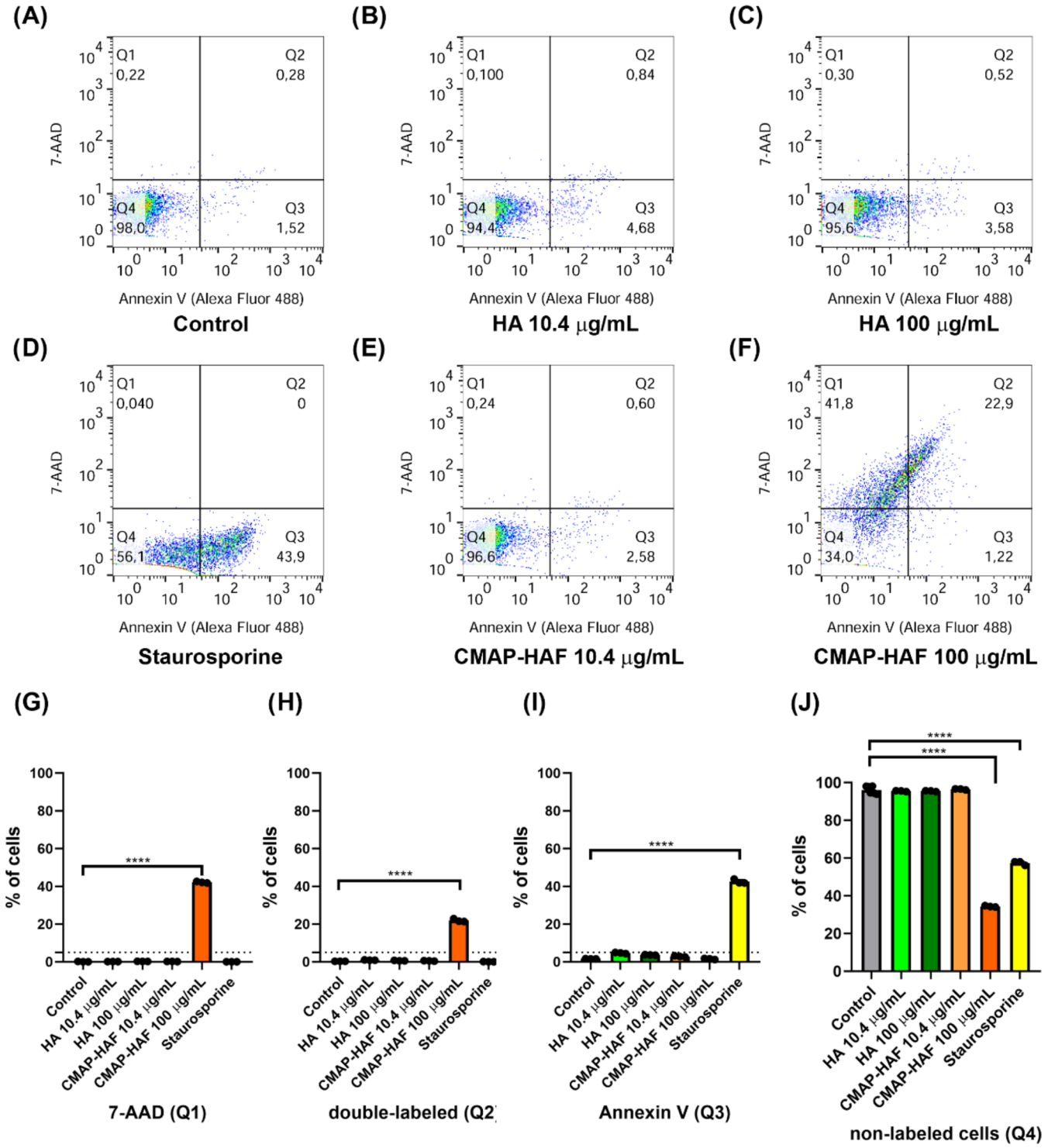

Figure 6. Only high doses of CMAP-HAF induce cytotoxicity in HDFa cells. HDFa cells were incubated with 7-AAD and annexin V and analyzed using flow cytometry. (A−F) Cells stained with 7-AAD but not with Annexin-V dye are necrotic cells, and they are presented in quadrant Q1 (top left). Cells that stained positive for Annexin-V and 7-AAD were necrotic and apoptotic, quadrant Q2 (top right). Cells stained with Annexin V and not with 7-AAD were apoptotic cells (quadrant Q3, bottom right). Cells that did not stain with either 7-AAD or Annexin-V dye were nonapoptotic and non-necrotic (live cells) in quadrant Q4 (bottom left). (G−J) Graphs quantifying the percentage of events in each quadrant. Each experiment was performed in triplicate. The graphs represent three independent experiments (**** $p < 0.0001$).

mainly labeled with 7-AAD (Figure 5E−G). In Figure 5E−G, it is possible to observe an increase in 7-AAD positive cells of 20.46 ± 0.39% treated with 10.4 μg mL^{-1} of CMAP-HAF and an increase of 76.06 ± 0.39% with 100 μg mL^{-1} of CMAP-HAF ($p < 0.0001$). Staurosporine (10 μM) was used as a positive control to induce apoptosis and showed an increase of 1.65 ± 0.34% compared with the untreated control group ($p < 0.0001$) (Figure 5D,I).

The same treatments were performed on HDFa cells. First, cells untreated with HA did not exhibit Annexin-V Alexa-488

https://doi.org/10.1021/acsanm.4c02467
ACS Appl. Nano Mater. 2024, 7, 21304−21318

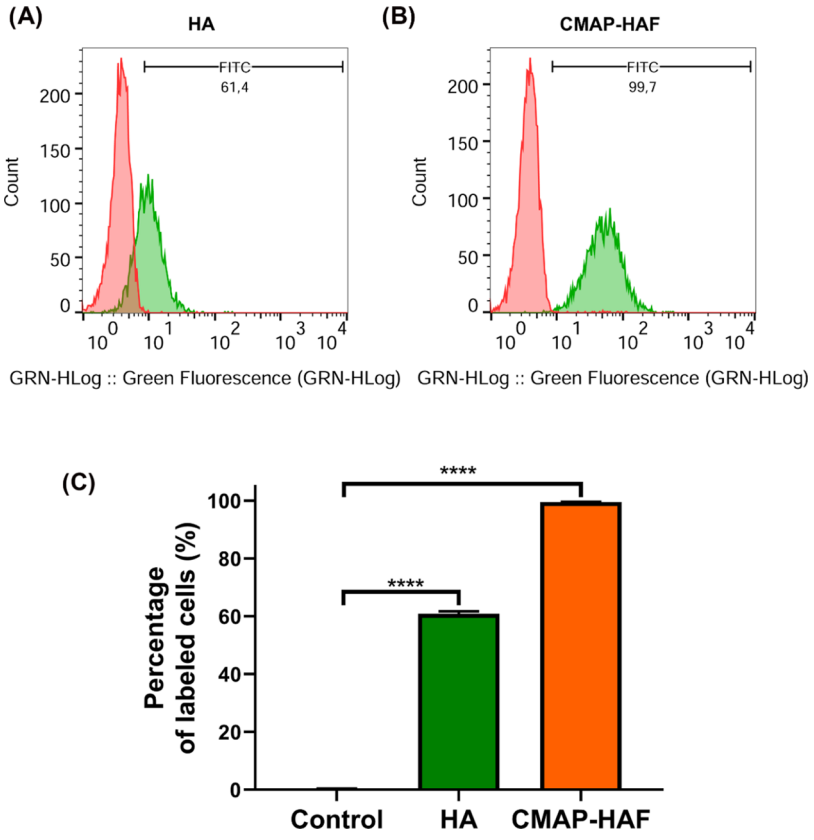

Figure 7. HA and CMAP-HAF could be internalized by U2OS. HA and CMAP-HAF FITC-conjugated were incubated with U2OS cells for 24 h. The percentage of cells bound to the FITC-conjugated nanomaterials was analyzed by flow cytometry. (A, B) The histograms presented in red are unlabeled cells, and the cells bonded to HA-FITC or CMAP-HAF-FITC are shown in green. (C) Graph quantifying the percentage of cells labeled with HA-FITC or CMAP-HAF-FITC. Each experiment was performed in triplicate.

or 7-AAD labeling (Figure 6A). Next, we observed an increase in 7-AAD of 42.05 ± 0.14% using 100 μg mL^{-1} of CMAP-HAF ($p < 0.0001$) (Figure 6E,G). The double-labeled data showed an increase of 21.63 ± 0.28% only with 100 μg mL^{-1} CMAP-HAF ($p < 0.0001$), demonstrating early apoptosis followed by a late necrosis event (Figure 6F,H). HDFa cells treated with HA were not labeled with Annexin-V Alexa-488 or 7-AAD (Figure 6B,C,6G−I). Staurosporine (500 nM) was used as a positive control to induce apoptosis and showed an increase of 40.94 ± 0.43% ($p < 0.0001$) (Figure 6D,I).

Together, these results suggest that 100 μg mL^{-1} of CMAP-HAF could compromise plasma membrane integrity in both cell types, causing necrosis. However, more double-labeled cells were observed in HDFa cells treated with 100 μg mL^{-1} CMAP-HAF. This result suggests that this concentration of CMAP-HAF triggers an early apoptotic event only in HDFa cells. Necrosis was observed only in U2OS cells upon exposure to 10 or 100 μg mL^{-1} of CMAP-HAF. This result confirms the observations of cell counting and MTT assay, showing a potent effect of CMAP-HAF on this cell line (Figure 3).

Curcumin induces apoptosis and necrosis in colorectal cancer organoids by inhibiting ERK phosphorylation[59] Furthermore, the combination of CM and FA has been shown to improve bioavailability and efficacy in the treatment of some diseases.[51] Apoptosis is a natural defense mechanism against cancer.[60] However, the ability of cancer cells to evade and resist apoptosis is a defining characteristic of the disease, often leading to tumor formation and drug resistance, resulting in chemotherapy failure.[61] Therefore, it is not only crucial to find ways to overcome this resistance to apoptosis but also to develop methods to trigger other forms of programmed cell death as alternative treatments for cancer. This study presents a new system featuring CMAP-HA functionalized with folic acid (CMAP-HAF). Thus, CMAP-HAF may be a promising candidate for OS treatment.

3.8. Cellular Uptake of Nanomaterials by Microscopy.

Flow cytometry and immunofluorescence were used to investigate the internalization of the nanocomposites in U2OS and HDFa cells. The cells were incubated with HA or CMAP-HAF conjugated to FITC (100 μg/mL^{-1}) overnight. Next, cells were analyzed using flow cytometry. Representative histograms showing the percentage of fluorescent U2OS cells in green (Figure 7A,B). Figure 7C shows the percentage of labeled cells, 60.9 ± 0.9% for HA and 99.6 ± 0.1% for CMAP-HAF, respectively. HA has a stable chemical structure, which means that it does not easily react with other substances. In addition, HA has a few reactive functional groups that can interact with other organic groups. These characteristics may limit the ability of HA to bind to other molecules, such as FITC, which could explain the lower conjugation observed in our experiment.[62]

Immunofluorescence was performed to detect α-tubulin (red) to confirm nanomaterial localization and internalization into the intracellular compartment. Next, serial z-section images were obtained to test the internalization of nanoparticles labeled with FITC (green). To confirm the nanocomposite cellular uptake, three-dimensional (3D) orthogonal projections were used (Figure 8A−E). The *xy*

https://doi.org/10.1021/acsanm.4c02467
ACS Appl. Nano Mater. 2024, 7, 21304−21318

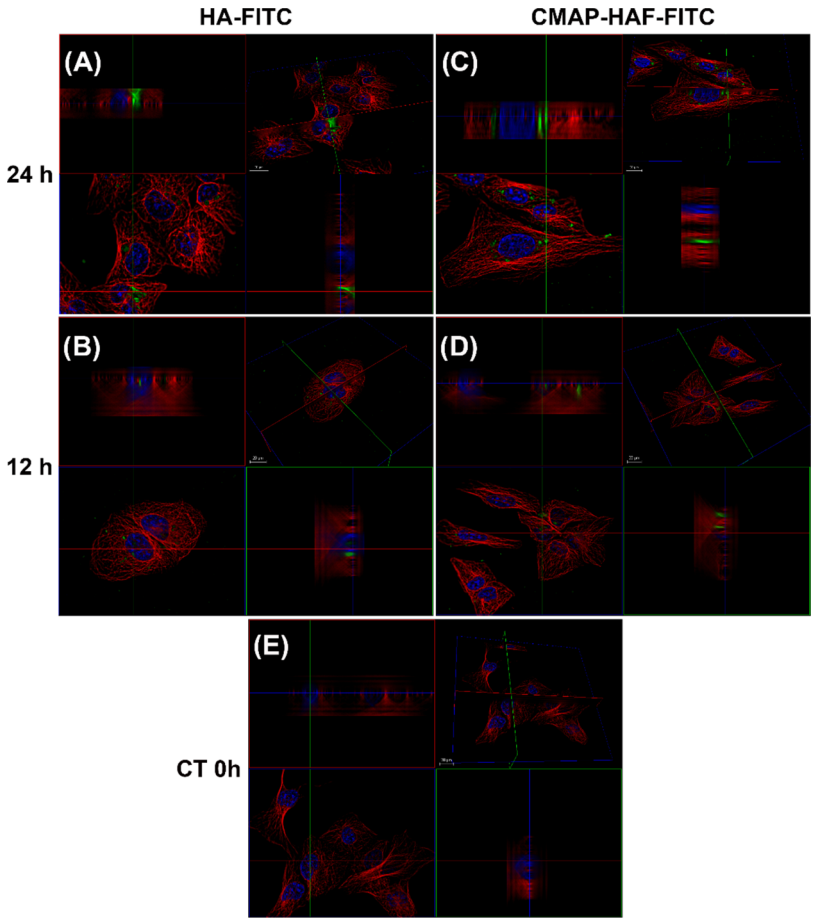

Figure 8. HA-FITC and CMAP-HAF-FITC nanoparticles were internalized by U2OS cells. Representative immunofluorescence images: (A, B) HA-FITC labeling is green, α-tubulin labeling is red, and nuclei are stained blue with Hoechst. (C, D) CMAP-HAF-FITC is in green, α-tubulin labeling is in red, and nuclei are stained in blue with Hoechst. (E) Control group (untreated). The cells were exposed to nanomaterials for 0, 12, and 24 h. Orthogonal three-dimensional (3D) reconstruction sections were used to demonstrate nanomaterial internalization. The red, green and blue lines indicate the *x*-, *y*-, and *z*-axes, respectively. Scale bars = 20 μm. Each experiment was performed in triplicate.

and *xz* projections showed that HA-FITC and CMAP-HAF-FITC accumulated in the intracellular and perinuclear regions of U2OS cells (Figure 8A–E).

Previous work has reported that the CM nanoformulation penetrated breast cancer cells (4T1) and showed the antiproliferative potential of CM. Additionally, nanocurcumin inhibits tumor growth in Balb/c mice by regulating genes involved in apoptosis and metastasis.[63] Curcumin is reported to have low bioavailability due to its poor solubility, permeability and absorption.[53,64] Furthermore, nanoencapsulation of CM significantly improves drug solubility, stability, cellular uptake, circulation time, and bioavailability in cancer cells.[53] Another group demonstrated that cellulose nanocrystals (CNCs) used as nanocarriers loaded with CM and FA improved the solubility and stability of CM.[64] Reported rod-like HA nanoparticles have a considerable advantage over spherical nanoparticles in cellular uptake.[65] The process of nanoparticle endocytosis begins with their interaction with the cell membrane. Given the abundance of receptors on the cell membrane, some of which exhibit high calcium affinity, nanoparticle uptake onto the cellular membrane can trigger cellular modifications.[66] Some authors have observed a strong correlation between cellular toxicity and the cellular uptake of nanomaterials.[11,65] Our findings demonstrated that CMAP-HAF was highly internalized by U2OS and HDFa cells. Therefore, the use of nanomaterials with improved cellular uptake is a promising option for enhancing the efficacy of cancer treatments, improving drug delivery, and potentially reducing side effects. However, further research is needed to fully understand the mechanisms of nanomaterial cellular uptake and to optimize their use in clinical applications.

3.9. Effects of HA and CMAP-HAF on U2OS Cell Migration. The migration of cells treated with HA or CMAP-HAF was compared using a wound healing assay. U2OS cells were cultured in DMEM for 24 h and treated with nanoparticles (100 $\mu g/mL^{-1}$) for another 24 h. Representative images were obtained at time points of 0, 24, and 48 h at identical locations; the quantification results are shown in Figure 9A. A significant decrease in wound closure was detected in cells exposed to CMAP-HAF compared to the untreated control group (Figure 9B, $p < 0.0001$). There was no difference between the untreated control and HA groups. In addition to inhibiting cell viability, our study showed that nano-CMAP-HAF treatment could prevent U2OS cell migration. The clonogenic survival assay was performed in U2OS cells after HA or CMAP-HAF treatment (10.4 or 100 $\mu g\ mL^{-1}$) then allowed to recover in fresh media for 10 days. Compared with the control group, there was a decrease in U2OS colony formation after EC_{50} treatment ($p < 0,05$) and no colony formation was observed at higher concentrations,

https://doi.org/10.1021/acsanm.4c02467
ACS Appl. Nano Mater. 2024, 7, 21304−21318

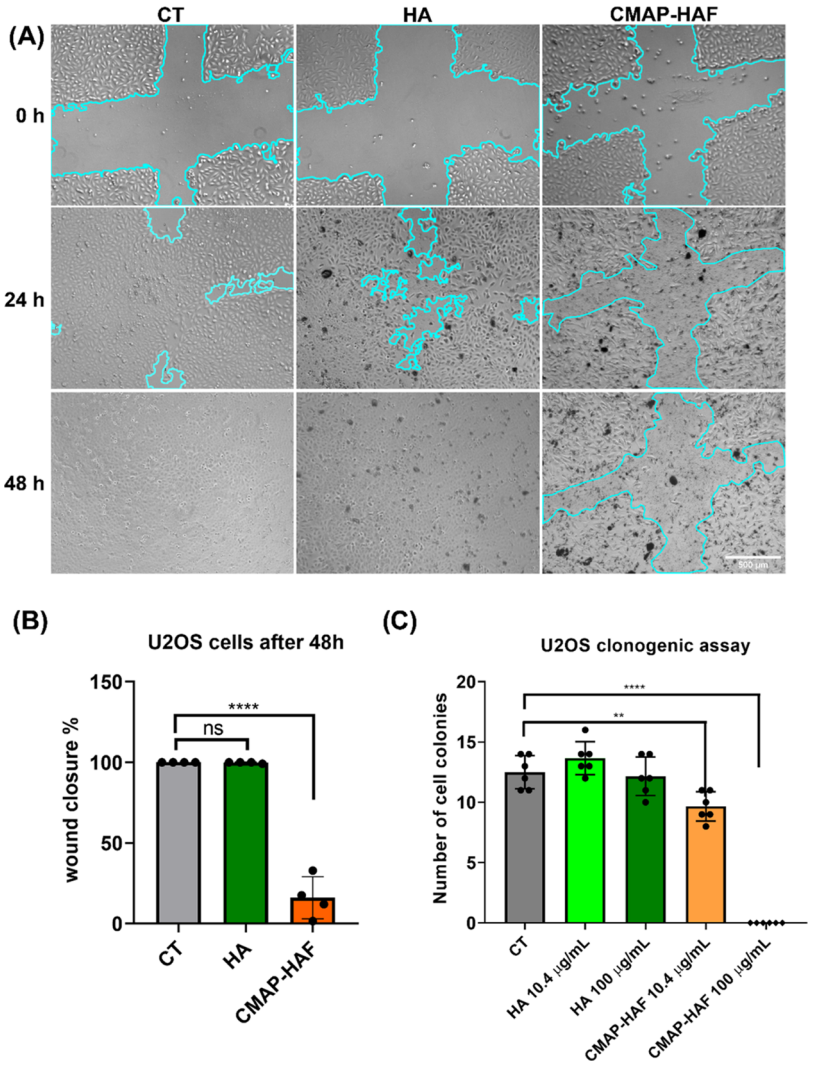

Figure 9. A higher dose of CMAP-HAF inhibited cell migration. Cells were wounded and stimulated with HA or CMAP-HAF (100 $\mu g/mL^{-1}$). (A) Representative bright-field images of the cell monolayer captured using a 4× objective lens. (B) Quantification of the wound closure %. Cyan areas represent spaces without cells. Scale bar = 500 μm. (C) Cells were exposed to HA or CMAP-HAF and cell viability was assessed using a clonogenic assay. (n = 3, ** p < 0.01, **** p < 0.0001).

which corroborates the migration assay findings (Figure 9C; p < 0.0001).

In recent decades, significant advancements in OS therapy have been limited by local recurrence and development of distant metastasis.[5] Cell migration is a key factor in the progression of metastatic tumors. Moreover, nanomaterials, including CM, have been reported to inhibit the growth of OS cell lines by inhibiting their migration.[67] Folic acid functionalization delays cell migration by promoting higher cellular internalization and target specificity in triple-negative breast cancer cells (TNBC).[68] The results showed that CMAP-HAF inhibited the migration of the U2OS cells. This study found that treating U2OS cells with nano-CMAP-HAF significantly inhibited cell migration and cloning formation. This finding is significant since cell migration plays a crucial role in the metastatic progression of tumors.[14] Despite no marked improvements in OS therapy in recent decades due to local recurrence or distant metastasis, the results suggest that nanomaterials such as CMAP-HAF could potentially be used to inhibit the growth and migration of OS cell lines, thereby offering a new option for OS therapy. However, further research is necessary to confirm these findings and investigate their clinical implications.

4. CONCLUSIONS

Osteosarcoma treatment remains challenging, and there has been limited improvement in patient survival rates for this aggressive type of bone cancer. Various chemotherapeutic agents have been employed to treat OS. However, these drugs often lead to toxicity and side effects and frequently result in chemoresistance. Given these challenges, this study introduces a novel approach for OS treatment using CMAP-HA functionalized with folic acid (CMAP-HAF). The successful incorporation of FA into the nanostructure presented characteristics that allowed its use as a drug carrier, as demonstrated by greater internalization in cell uptake assays. These results indicate that CMAP-HAF decreased cyclin E expression, compromised plasma membrane integrity, leading to late necrosis and impacting cell migration. These results highlight the potential of CMAP-HAF as a promising therapeutic agent in cancer treatment. This innovative

https://doi.org/10.1021/acsanm.4c02467
ACS Appl. Nano Mater. 2024, 7, 21304−21318

approach may enhance future patient management strategies for OS.

■ ASSOCIATED CONTENT

Data Availability Statement

The data will be made available upon request.

Supporting Information

The Supporting Information is available free of charge at https://pubs.acs.org/doi/10.1021/acsanm.4c02467.

The control group HA cell viability was assessed by MTT assay and nuclear cell counting by Hoechst staining (Figure S1A−C); representative images of HDFa and U2OS cells after CMAP-HAF treatment (Figures S2 and S3); the IC_{50} representative graph (Figure S4); ROS production was assayed using carboxy-H2DCFDA (Figure S5A−D) (PDF)

■ AUTHOR INFORMATION

Corresponding Author

Edésia Martins Barros de Sousa − *Centro de Desenvolvimento da Tecnologia Nuclear − CDTN, 31270-901 Belo Horizonte, Minas Gerais, Brazil;* orcid.org/0000-0002-6317-4054; Phone: +55 (31) 3439-9523; Email: sousaem@cdtn.br

Authors

Michele Angela Rodrigues − *Centro de Desenvolvimento da Tecnologia Nuclear − CDTN, 31270-901 Belo Horizonte, Minas Gerais, Brazil;* orcid.org/0000-0002-0233-7729

Jéssica Pauline Nunes Marinho − *Centro de Desenvolvimento da Tecnologia Nuclear − CDTN, 31270-901 Belo Horizonte, Minas Gerais, Brazil;* orcid.org/0000-0002-1717-6323

Luísa Arantes Fernandes Vieira − *Centro de Desenvolvimento da Tecnologia Nuclear − CDTN, 31270-901 Belo Horizonte, Minas Gerais, Brazil;* orcid.org/0009-0001-2044-0092

Dawidson Assis Gomes − *Departamento de Bioquímica e Imunologia, Instituto de Ciências Biológicas, Universidade Federal de Minas Gerais - UFMG, 31270-901 Belo Horizonte, Minas Gerais, Brazil;* orcid.org/0000-0001-7714-991X

Complete contact information is available at: https://pubs.acs.org/10.1021/acsanm.4c02467

Author Contributions

M.A.R.: conceptualization, methodology, validation, investigation and writing—original draft, writing— review and editing. J.P.N.M.: conceptualization, methodology, validation, investigation and writing—original draft. L.A.F.V.: Methodology, validation, investigation. D.A.G.: Methodology, validation, investigation and writing—original draft, writing— review and editing. E.M.B.S.: Conceptualization, validation, writing—review and editing, resources, supervision, funding acquisition.

Notes

The authors declare no competing financial interest.

■ ACKNOWLEDGMENTS

The authors would like to thank Fundação de Amparo à Pesquisa do Estado de Minas Gerais (FAPEMIG; APQ-01987-23; APQ-03132-18), Coordenação de Aperfeiçoamento de Pessoal de Nível Superior (CAPES), Rede Mineira de Engenharia de Tecidos e Terapia Celular (REMETTEC; RED00213-23; FAPEMIG), Rede Mineira de Pesquisa Translational em Oncologia (RED00059-23; FAPEMIG), Conselho Nacional de Desenvolvimento Científico e Tecnológico (CNPq; 304061/2022-0, 307998/2022−3; 442098/2023−5), National Institutes of Health (NIH; grant 1R03TW008709) and Financiadora de Estudos e Projetos (FINEP; 29374) to support this work. The authors also thank "*Centro de Microscopia*" (CM-UFMG) and "*Centro de Aquisição e Processamento de Imagens*" (CAPI-ICB/UFMG) for technical support.

■ REFERENCES

(1) Zahedipour, F.; Bolourinezhad, M.; Teng, Y.; Sahebkar, A. The Multifaceted Therapeutic Mechanisms of Curcumin in Osteosarcoma: State-of-the-Art. *J. Oncol.* **2021**, *2021*, No. 3006853, DOI: 10.1155/2021/3006853.

(2) Smoke, A.; Anderson, P. M.; Gulia, A.; Gennatas, S.; Huang, P. H.; Jones, R. L. Future Directions in the Treatment of Osteosarcoma. *Cells* **2021**, *10*, No. 172, DOI: 10.3390/cells10010172.

(3) Xu, C.; Wang, M.; Guo, W.; Sun, W.; Liu, Y. Curcumin in Osteosarcoma Therapy: Combining With Immunotherapy, Chemotherapeutics, Bone Tissue Engineering Materials and Potential Synergism With Photodynamic Therapy. *Front. Oncol.* **2021**, *11*, No. 672490, DOI: 10.3389/fonc.2021.672490.

(4) Kansara, M.; Teng, M. W.; Smyth, M. J.; Thomas, D. M. Translational Biology of Osteosarcoma. *Nat. Rev. Cancer* **2014**, *14*, 722−735, DOI: 10.1038/nrc3838.

(5) Wang, R.; Liu, W.; Wang, Q.; Li, G.; Wan, B.; Sun, Y.; Niu, X.; Chen, D.; Tian, W. Anti-Osteosarcoma Effect of Hydroxyapatite Nanoparticles Both: In Vitro and in Vivo by Downregulating the FAK/PI3K/Akt Signaling Pathway. *Biomater. Sci.* **2020**, *8* (16), 4426−4437.

(6) Ielo, I.; Calabrese, G.; De Luca, G.; Conoci, S. Recent Advances in Hydroxyapatite-Based Biocomposites for Bone Tissue Regeneration in Orthopedics. *Int. J. Mol. Sci.* **2022**, *23*, No. 9721, DOI: 10.3390/ijms23179721.

(7) Zhang, Y.; Zheng, N.; Cao, Y.; Wang, F.; Wang, P.; Ma, Y.; Lu, B.; Hou, G.; Fang, Z.; Liang, Z.; Yue, M.; Li, Y.; Chen, Y.; Fu, J.; Wu, J.; Xie, T.; Feng, X. Climbing-Inspired Twining Electrodes Using Shape Memory for Peripheral Nerve Stimulation and Recording. *Sci. Adv.* **2019**, *5* (4), No. eaaw1066.

(8) Guo, X.; Xue, M.; Chen, F.; Guo, Q.; Zhou, X.; Lin, H.; Chen, Y. Local Delivery and Controlled Release of MiR-34a Loaded in Hydroxyapatite/Mesoporous Organosilica Nanoparticles Composite-Coated Implant Wire to Accelerate Bone Fracture Healing. *Biomaterials* **2022**, *280*, No. 121300.

(9) Qing, F.; Wang, Z.; Hong, Y.; Liu, M.; Guo, B.; Luo, H.; Zhang, X. Selective Effects of Hydroxyapatite Nanoparticles on Osteosarcoma Cells and Osteoblasts. *J. Mater. Sci.: Mater. Med.* **2012**, *23* (9), 2245−2251.

(10) Wu, H.; Li, Z.; Tang, J.; Yang, X.; Zhou, Y.; Guo, B.; Wang, L.; Zhu, X.; Tu, C.; Zhang, X. The in Vitro and in Vivo Anti-Melanoma Effects of Hydroxyapatite Nanoparticles: Influences of Material Factors. *Int. J. Nanomed.* **2019**, *14*, 1177−1191.

(11) Cui, X.; Liang, T.; Liu, C.; Yuan, Y.; Qian, J. Correlation of Particle Properties with Cytotoxicity and Cellular Uptake of Hydroxyapatite Nanoparticles in Human Gastric Cancer Cells. *Mater. Sci. Eng., C* **2016**, *67*, 453−460.

(12) Guo, G.; Tian, A.; Lan, X.; Fu, C.; Yan, Z.; Wang, C. Nano Hydroxyapatite Induces Glioma Cell Apoptosis by Suppressing NF-κB Signaling Pathway. *Exp. Ther. Med.* **2019**, *17*, 4080−4088.

(13) Nguyen, T.; Maniyar, A.; Sarkar, M.; Sarkar, T. R.; Neelgund, G. M. The Cytotoxicity of Carbon Nanotubes and Hydroxyapatite, and Graphene and Hydroxyapatite Nanocomposites against Breast Cancer Cells. *Nanomaterials* **2023**, *13* (3), No. 556.

(14) Yang, Z. J.; Huang, S. Y.; Zhou, D. D.; Xiong, R. G.; Zhao, C. N.; Fang, A. P.; Zhang, Y. J.; Li, H. B.; Zhu, H. L. Effects and

Mechanisms of Curcumin for the Prevention and Management of Cancers: An Updated Review. *Antioxidants* **2022**, *11*, No. 1481, DOI: 10.3390/antiox11081481.
(15) Giordano, A.; Tommonaro, G. Curcumin and Cancer. *Nutrients* **2019**, *11*, No. 2376, DOI: 10.3390/nu11102376.
(16) Ghasemi, F.; Shafiee, M.; Banikazemi, Z.; Pourhanifeh, M. H.; Khanbabaei, H.; Shamshirian, A.; Moghadam, S. A.; ArefNezhad, R.; Sahebkar, A.; Avan, A.; Mirzaei, H. Curcumin Inhibits NF-KB and Wnt/β-Catenin Pathways in Cervical Cancer Cells. *Pathol., Res. Pract.* **2019**, *215* (10), No. 152556.
(17) Li, H.; Yue, L.; Xu, H.; Li, N.; Li, J.; Zhang, Z.; Zhao, R. C. Correction for: Curcumin Suppresses Osteogenesis by Inducing MiR-126a-3p and Subsequently Suppressing the WNT/LRP6 Pathway. *Aging* **2021**, *13* (6), 9152−9153.
(18) Lu, K. H.; Lu, P. W. A.; Lu, E. W. H.; Lin, C. W.; Yang, S. F. Curcumin and Its Analogs and Carriers: Potential Therapeutic Strategies for Human Osteosarcoma. *Int. J. Biol. Sci.* **2023**, *19*, 1241−1265, DOI: 10.7150/ijbs.80590.
(19) Thulasidasan, A. K. T.; Retnakumari, A. P.; Shankar, M.; Vijayakurup, V.; Anwar, S.; Thankachan, S.; Pillai, K. S.; Pillai, J. J.; Nandan, C. D.; Alex, V. V.; Chirayil, T. J.; Sundaram, S.; Kumar, G. S. V.; Anto, R. J. Folic Acid Conjugation Improves the Bioavailability and Chemosensitizing Efficacy of Curcumin-Encapsulated PLGA-PEG Nanoparticles towards Paclitaxel Chemotherapy. *Oncotarget* **2017**, *8*, 107374−107389, DOI: 10.18632/oncotarget.22376.
(20) Guo, X.; Mei, J.; Jing, Y.; Wang, S. Curcumin-Loaded Nanoparticles with Low-Intensity Focused Ultrasound-Induced Phase Transformation as Tumor-Targeted and PH-Sensitive Theranostic Nanoplatform of Ovarian Cancer. *Nanoscale Res. Lett.* **2020**, *15* (1), No. 73, DOI: 10.1186/s11671-020-03302-3.
(21) Cipreste, M. F.; Gonzalez, I.; da Mata Martins, T. M.; Goes, A. M.; de Almeida Macedo, W. A.; de Sousa, E. M. B. Attaching Folic Acid on Hydroxyapatite Nanorod Surfaces: An Investigation of the HA-FA Interaction. *RSC Adv.* **2016**, *6* (80), 76390−76400.
(22) Marinho, J. P. N.; Neme, N. P.; de Souza Matos, M. J.; Batista, R. J. C.; de Almeida Macedo, W. A.; Gastelois, P. L.; Gomes, D. A.; Rodrigues, M. A.; Cipreste, M. F.; de Sousa, E. M. B. Nanostructured System Based on Hydroxyapatite and Curcumin: A Promising Candidate for Osteosarcoma Therapy. *Ceram. Int.* **2023**, *49* (12), 19932−19949.
(23) da Costa Januário Meireles, I. B.; Cipreste, M. F.; Gastelois, P. L.; de Almeida Macedo, W. A.; Gomes, D. A.; de Sousa, E. M. B. Synthesis and Characterization of Gold Nanorods Coated by Mesoporous Silica MCM-41 as a Platform for Bioapplication in Photohyperthermia. *Nanotechnology* **2021**, *32* (50), No. 505720.
(24) Vieira, L. A. F.; Marinho, J. P. N.; Rodrigues, M. A.; de Souza, J. P. B.; de Sousa, R. G.; de Sousa, E. M. B. Nanocomposite Based on Hydroxyapatite and Boron Nitride Nanostructures Containing Collagen and Tannic Acid Ameliorates the Mechanical Strengthening and Tumor Therapy. *Ceram. Int.* **2024**, *50* (18), 32064−32080.
(25) Grishagin, I. V. Automatic Cell Counting with ImageJ. *Anal. Biochem.* **2015**, *473*, 63−65.
(26) Gao, F.; Liang, W.; Chen, Q.; Chen, B.; Liu, Y.; Liu, Z.; Xu, X.; Zhu, R.; Cheng, L. A Curcumin-Decorated Nanozyme with ROS Scavenging and Anti-Inflammatory Properties for Neuroprotection. *Nanomaterials* **2024**, *14* (5), No. 389.
(27) de Miranda, M. C.; Rodrigues, M. A.; de Angelis Campos, A. C.; Faria, J. A. Q. A.; Kunrath-Lima, M.; Mignery, G. A.; Schechtman, D.; Goes, A. M.; Nathanson, M. H.; Gomes, D. A. Epidermal Growth Factor (EGF) Triggers Nuclear Calcium Signaling through the Intranuclear Phospholipase C-4 (PLC4). *J. Biol. Chem.* **2019**, *294* (45), 16650−16662.
(28) Kumar, G.; Degheidy, H.; Casey, B. J.; Goering, P. L. Flow Cytometry Evaluation of in Vitro Cellular Necrosis and Apoptosis Induced by Silver Nanoparticles. *Food Chem. Toxicol.* **2015**, *85*, 45−51.
(29) Dantas, A. E.; Horta, C. C. R.; Martins, T. M. M.; do Carmo, A. O.; de Oliveira Mendes, B. B. R.; Goes, A. M.; Kalapothakis, E.; Gomes, D. A. Whole Venom of Loxosceles Similis Activates Caspases-3, −6, −7, and −9 in Human Primary Skin Fibroblasts. *Toxicon* **2014**, *84*, 56−64.
(30) Rodrigues, M. A.; Gomes, D. A.; Cosme, A. L.; Sanches, M. D.; Resende, V.; Cassali, G. D. Inositol 1,4,5-Trisphosphate Receptor Type 3 (ITPR3) Is Overexpressed in Cholangiocarcinoma and Its Expression Correlates with S100 Calcium-Binding Protein A4 (S100A4). *Biomed. Pharmacother.* **2022**, *145*, No. 112403.
(31) Faria, J. A. Q. A.; de Andrade, C.; Goes, A. M.; Rodrigues, M. A.; Gomes, D. A. Effects of Different Ligands on Epidermal Growth Factor Receptor (EGFR) Nuclear Translocation. *Biochem. Biophys. Res. Commun.* **2016**, *478* (1), 39−45.
(32) Martinotti, S.; Ranzato, E.Scratch Wound Healing Assay. In *Methods in Molecular Biology*; Springer, 2019; Vol. *2109*, pp 225−229.
(33) Suarez-Arnedo, A.; Figueroa, F. T.; Clavijo, C.; Arbeláez, P.; Cruz, J. C.; Muñoz-Camargo, C. An Image J Plugin for the High Throughput Image Analysis of in Vitro Scratch Wound Healing Assays. *PLoS One* **2020**, *15* (7), No. e0232565.
(34) Ronson, G. E.; Piberger, A. L.; Higgs, M. R.; Olsen, A. L.; Stewart, G. S.; McHugh, P. J.; Petermann, E.; Lakin, N. D. PARP1 and PARP2 Stabilise Replication Forks at Base Excision Repair Intermediates through Fbh1-Dependent Rad51 Regulation. *Nat. Commun.* **2018**, *9* (1), No. 746.
(35) Chen, L.; Mccrate, J. M.; Lee, J. C. M.; Li, H. The Role of Surface Charge on the Uptake and Biocompatibility of Hydroxyapatite Nanoparticles with Osteoblast Cells. *Nanotechnology* **2011**, *22* (10), No. 105708.
(36) Wu, J. The Enhanced Permeability and Retention (Epr) Effect: The Significance of the Concept and Methods to Enhance Its Application. *J. Pers. Med.* **2021**, *11*, No. 771, DOI: 10.3390/jpm11080771.
(37) dos Apostolos, R. C. R.; Cipreste, M. F.; de Sousa, R. G.; de Sousa, E. M. B. Multifunctional Hybrid Nanosystems Based on Mesoporous Silica and Hydroxyapatite Nanoparticles Applied as Potential Nanocarriers for Theranostic Applications. *J. Nanopart. Res.* **2020**, *22* (12), No. 368, DOI: 10.1007/s11051-020-05105-0.
(38) Vieira, L. A. F.; da Costa Januário Meireles, I. B.; Sousa, E. M. B. Boron Nitride Nanostructures Reinforced Nanohydroxyapatite: Bifunctional Nanocomposite for Potential Orthopedical Use and Ciprofloxacin Controlled Delivery. *J. Ceram. Process. Res.* **2022**, *23* (5), 725−736.
(39) Cipreste, M. F.; Peres, A. M.; Cotta, A. A. C.; Aragón, F. H.; de M Antunes, A.; Leal, A. S.; Macedo, W. A. A.; de Sousa, E. M. B. Synthesis and Characterization of 159Gd-Doped Hydroxyapatite Nanorods for Bioapplications as Theranostic Systems. *Mater. Chem. Phys.* **2016**, *181*, 301−311.
(40) Song, X.; Liu, X.; Ma, Y.; Zhu, Q.; Bi, M. Synthesis of Ce/Gd@HA/PLGA Scaffolds Contributing to Bone Repair and MRI Enhancement. *Front. Bioeng. Biotechnol.* **2022**, *10*, No. 834226.
(41) Jose, S.; Senthilkumar, M.; Elayaraja, K.; Haris, M.; George, A.; Raj, A. D.; Sundaram, S. J.; Bashir, A. K. H.; Maaza, M.; Kaviyarasu, K. Preparation and Characterization of Fe Doped N-Hydroxyapatite for Biomedical Application. *Surf. Interfaces* **2021**, *25*, No. 101185.
(42) Sivakumar, P. M.; Yetisgin, A. A.; Sahin, S. B.; Demir, E.; Cetinel, S. Enhanced Properties of Nickel−Silver Codoped Hydroxyapatite for Bone Tissue Engineering: Synthesis, Characterization, and Biocompatibility Evaluation. *Environ. Res.* **2023**, *238* (P2), No. 117131.
(43) Lee, W. H.; Rohanizadeh, R.; Loo, C. Y. In Situ Functionalizing Calcium Phosphate Biomaterials with Curcumin for the Prevention of Bacterial Biofilm Infections. *Colloids Surf., B* **2021**, *206*, No. 111938.
(44) Verma, G.; Gajipara, A.; Shelar, S. B.; Priyadarsini, K. I.; Hassan, P. A. Development of Water-Dispersible Gelatin Stabilized Hydroxyapatite Nanoformulation for Curcumin Delivery. *J. Drug Delivery Sci. Technol.* **2021**, *66*, No. 102769.
(45) Hu, K.; Huang, X.; Gao, Y.; Huang, X.; Xiao, H.; McClements, D. J. Core-Shell Biopolymer Nanoparticle Delivery Systems: Synthesis and Characterization of Curcumin Fortified Zein-Pectin Nanoparticles. *Food Chem.* **2015**, *182*, 275−281.

(46) Fahmi, M. Z.; Sholihah, N. F.; Wibrianto, A.; Sakti, S. C. W.; Firdaus, F.; Chang, J. y. Simple and Fast Design of Folic Acid-Based Carbon Dots as Theranostic Agent and Its Drug Release Aspect. *Mater. Chem. Phys.* **2021**, *267*, No. 124596.
(47) Mohammed, A. S. Y.; Dyab, A. K. F.; Taha, F.; El-Mageed, A. I. A. A. Encapsulation of Folic Acid (Vitamin B9) into Sporopollenin Microcapsules: Physico-Chemical Characterisation, in Vitro Controlled Release and Photoprotection Study. *Mater. Sci. Eng., C* **2021**, *128*, No. 112271.
(48) Narmani, A.; Rezvani, M.; Farhood, B.; Darkhor, P.; Mohammadnejad, J.; Amini, B.; Refahi, S.; Goushbolagh, N. A. Folic Acid Functionalized Nanoparticles as Pharmaceutical Carriers in Drug Delivery Systems. *Drug Dev. Res.* **2019**, *80* (4), 404−424.
(49) Rasmussen, M. K.; Pedersen, J. N.; Marie, R. Size and Surface Charge Characterization of Nanoparticles with a Salt Gradient. *Nat. Commun.* **2020**, *11* (1), No. 2337, DOI: 10.1038/s41467-020-15889-3.
(50) Yin, M.; Yin, Y.; Han, Y.; Dai, H.; Li, S. Effects of Uptake of Hydroxyapatite Nanoparticles into Hepatoma Cells on Cell Adhesion and Proliferation. *J. Nanomater.* **2014**, *2014*, No. 731897, DOI: 10.1155/2014/731897.
(51) Hussain, A.; Kumar, A.; Uttam, V.; Sharma, U.; Sak, K.; Saini, R. V.; Saini, A. K.; Haque, S.; Tuli, H. S.; Jain, A.; Sethi, G. Application of Curcumin Nanoformulations to Target Folic Acid Receptor in Cancer: Recent Trends and Advances. *Environ. Res.* **2023**, *233*, No. 116476, DOI: 10.1016/j.envres.2023.116476.
(52) Lee, W. H.; Rohanizadeh, R.; Loo, C. Y. In Situ Functionalizing Calcium Phosphate Biomaterials with Curcumin for the Prevention of Bacterial Biofilm Infections. *Colloids Surf., B* **2021**, *206*, No. 111938.
(53) Lee, W. H.; Loo, C. Y.; Rohanizadeh, R. Functionalizing the Surface of Hydroxyapatite Drug Carrier with Carboxylic Acid Groups to Modulate the Loading and Release of Curcumin Nanoparticles. *Mater. Sci. Eng., C* **2019**, *99*, 929−939.
(54) Radha, R.; Paul, V.; Anjum, S.; Bouakaz, A.; Pitt, W. G.; Husseini, G. A. Enhancing Curcumin's Therapeutic Potential in Cancer Treatment through Ultrasound Mediated Liposomal Delivery. *Sci. Rep.* **2024**, *14* (1), No. 10499.
(55) Matthews, H. K.; Bertoli, C.; de Bruin, R. A. M. Cell Cycle Control in Cancer. *Nat. Rev. Mol. Cell Biol.* **2022**, *23* (1), 74−88.
(56) Cavalu, S.; Abdelhamid, A. M.; Saber, S.; Elmorsy, E. A.; Hamad, R. S.; Abdel-Reheim, M. A.; Yahya, G.; Salama, M. M. Cell Cycle Machinery in Oncology: A Comprehensive Review of Therapeutic Targets. *FASEB J.* **2024**, *38* (11), No. e23734, DOI: 10.1096/fj.202400769R.
(57) Zhou, H.; Ning, Y.; Zeng, G.; Zhou, C.; Ding, X. Curcumin Promotes Cell Cycle Arrest and Apoptosis of Acute Myeloid Leukemia Cells by Inactivating AKT. *Oncol. Rep.* **2021**, *45* (4), No. 11.
(58) Brumatti, G.; Sheridan, C.; Martin, S. J. Expression and Purification of Recombinant Annexin V for the Detection of Membrane Alterations on Apoptotic Cells. *Methods* **2008**, *44* (3), 235−240.
(59) Elbadawy, M.; Hayashi, K.; Ayame, H.; Ishihara, Y.; Abugomaa, A.; Shibutani, M.; Hayashi, S. M.; Hazama, S.; Takenouchi, H.; Nakajima, M.; Tsunedomi, R.; Suzuki, N.; Nagano, H.; Shinohara, Y.; Kaneda, M.; Yamawaki, H.; Usui, T.; Sasaki, K. Anti-Cancer Activity of Amorphous Curcumin Preparation in Patient-Derived Colorectal Cancer Organoids. *Biomed. Pharmacother.* **2021**, *142*, No. 112043.
(60) Hanahan, D.; Weinberg, R. A. Hallmarks of Cancer: The next Generation. *Cell* **2011**, *144*, 646−674.
(61) Majidpoor, J.; Mortezaee, K. Steps in Metastasis: An Updated Review. *Med. Oncol.* **2021**, *38*, No. 3, DOI: 10.1007/s12032-020-01447-w.
(62) Bulina, N. V.; Makarova, S. V.; Baev, S. G.; Matvienko, A. A.; Gerasimov, K. B.; Logutenko, O. A.; Bystrov, V. S. A Study of Thermal Stability of Hydroxyapatite. *Minerals* **2021**, *11* (12), No. 1310.
(63) Kandjani, B. Z.; Hesari, F. S.; Babaei, E. Gemini Curcumin Inhibits 4T1 Cancer Cell Proliferation and Modulates the Expression of Apoptotic and Metastatic Genes in Balb/c Mice Model. *Pathol., Res. Pract.* **2023**, *243*, No. 154344.
(64) Cui, M.; Tian, Y.; Liu, Y.; Liu, H.; Tao, J. A Highly Therapeutic and Selective Delivery System for Curcumin Based on Nanocellulose and Folic Acid. *Cellulose* **2023**, *30* (8), 5113−5126.
(65) Motskin, M.; Wright, D. M.; Muller, K.; Kyle, N.; Gard, T. G.; Porter, A. E.; Skepper, J. N. Hydroxyapatite Nano and Microparticles: Correlation of Particle Properties with Cytotoxicity and Biostability. *Biomaterials* **2009**, *30* (19), 3307−3317.
(66) Lee, W. H.; Loo, C. Y.; Rohanizadeh, R. A Review of Chemical Surface Modification of Bioceramics: Effects on Protein Adsorption and Cellular Response. *Colloids Surf., B* **2014**, 823−834, DOI: 10.1016/j.colsurfb.2014.07.029.
(67) Walters, D. K.; Muff, R.; Langsam, B.; Born, W.; Fuchs, B. Cytotoxic Effects of Curcumin on Osteosarcoma Cell Lines. *Invest. New Drugs* **2008**, *26* (4), 289−297.
(68) De, A.; Roychowdhury, P.; Bhuyan, N. R.; Ko, Y. T.; Singh, S. K.; Dua, K.; Kuppusamy, G. Folic Acid Functionalized Diallyl Trisulfide−Solid Lipid Nanoparticles for Targeting Triple Negative Breast Cancer. *Molecules* **2023**, *28* (3), No. 1393.